PII: S0955-2219(98)00155-1

0955-2219/98/$—see front matter

Biomorphic Cellular Silicon Carbide Ceramics from Wood: II. Mechanical Properties

Peter Greil,* Thomas Lifka and Annette Kaindl

University of Erlangen-Nuernberg, Department of Materials Science, Glass and Ceramics, Martensstr. 5, D-91058 Erlangen, Germany

(Received 20 March 1998; accepted 16 June 1998)

Abstract

Silicon carbide ceramics with anisotropic pore microstructures pseudomorphous to wood were obtained by liquid Si infiltration of porous carbonized wood templates. Depending on the initial cellular microstructure of the various kinds of wood (ebony, beech, oak, maple, pine, balsa) ceramic materials of different density, pore structure and degree of anisotropy were obtained. Strength and elastic modulus of the pyrolyzed carbon preform and of the final silicon carbide ceramic were measured in different loading directions with respect to the initial cell orientation, e.g. axial, radial and tangential. Generally, the mechanical properties increase with fractional density. Strength and strain-to-failure in axial direction exhibit significantly higher values compared to loading in radial and tangential directions. The orientation dependence of microstructure-property relations may become important for the development of advanced anisotropic light weight structural materials.

1 Introduction

Manufacturing of ceramic materials from biological templates such as wood has become a matter of increasing interest because of the possibility of producing novel ceramic materials with a unique microstructure pseudomorphous to wood. Wood is a natural composite material with a hierarchical architecture where biopolymers such as cellulose, hemicellulose and lignin form a cellular microstructure of high porosity which, however, exhibits a remarkable combination of high strength, stiffness and toughness at low density.[1–3] The microstructural features of wood range from mm (growth ring patterns) via μm (tracheidal cell patterns, macro- and microfibril cell wall textures) down to nm scale (molecular cellulose fiber and membrane structures of cell walls). Figure 1 shows the macroscopic structure of wood with respect to the preferential cell orientation and examples of typical mesoscopic structures of softwood and hardwood.[4] While softwood is composed primarily of tracheidal (90 vol%) and parenchymal cells, the cellular microstructure of hardwood is more complex and contains additional libriformal cells. The tracheidal cells provide the transportation path for water, whereas the parenchymal cells are for storage and the libriformal cells for mechanical strengthening of wood. Typical dimensions for tracheidal cells in softwood are 30–50 μm in diameter and 2900–4500 μm in length and in deciduous wood 50–200 μm in diameter and 100–800 μm in length.

The mechanical behavior of wood is characterized by its pronounced anisotropy of elasticity and deformation behavior due to the anisotropic cellular structure. Strength, toughness and elastic modulus in axial direction are significantly higher compared to radial and tangential loading directions. The mechanical properties primarily depend on the macroscopic cellular structure, e.g. the morphology and orientation of the wood cells. For solid bodies with cellular pore structures various micromechanical models were derived which provide relationships between the fractional density (total density over cell wall material density), the cell wall material properties and the mechanical behavior of the porous solid body.[5–10] For highly porous bodies with a fractional density less than 0·3 an open cellular model (OCF) expresses the mechanical behavior (elasticity, tensile and compression strength, fracture toughness) as a function

*To whom correspondence should be addressed.

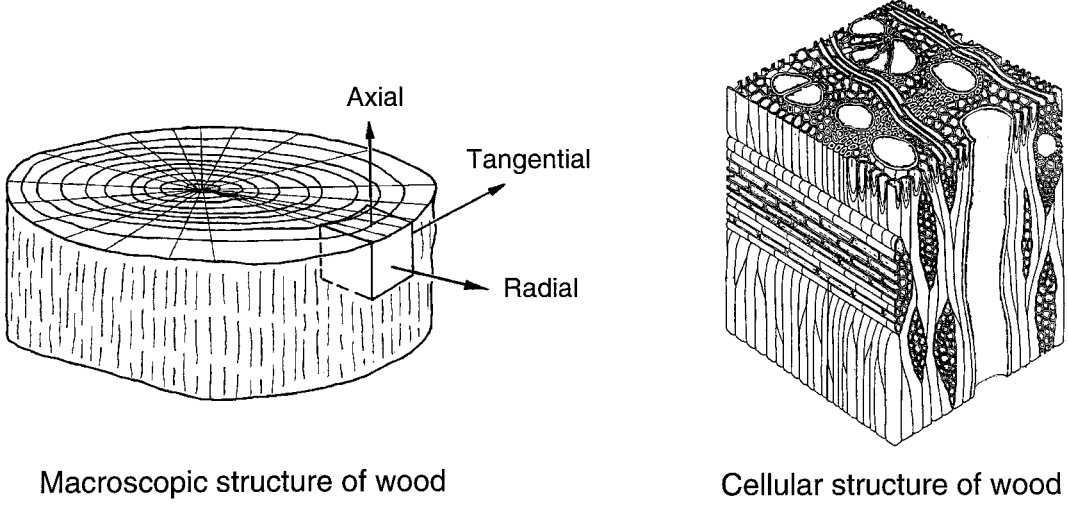

Fig. 1. Macroscopic cellular structure of wood.

of cell morphologies in a representative unit cell whereas a closed cellular model (CCF) accounts for cellular materials with a modified cell wall material distribution.

Generally, the OCF and CCF models predict an increasing degree of anisotropy with decreasing fractional density. On a microscopic level the orientation of the cellulose microfibrils forming the cell wall structure exert a strong influence. With increasing deviation of the microfibril orientation from the axial direction (deviation angle) strength was found to decrease signiflcantly whereas shrinkage during drying increased.[11,12] It is of particular interest if these macro- and microstructural features which determine the properties of natural wood also dominate the mechanical properties of ceramics with a cellular microstructure pseudomorphous to wood.

Silicon carbide materials with cellular microstructures derived from ebony, beech, oak, maple, pine, and balsa, respectively, were used to examine the mechanical behavior as a function of microstructure (fractional density) and loading orientation. Specimens were prepared with specific orientation of the initial cellular structure and examined for their elasticity, bending and compression strength and fracture behavior in different loading directions. The properties of the wood derived SiC was compared with conventional (isotropic) SiSiC processed by silicon infiltrated SiC powders.

2 Experimental Procedure

The biogenetic silicon carbide materials were produced by a liquid silicon melt infiltration and reaction process of carbonized preforms which were obtained by pyrolysis of wood. The processing is described in detail in part 1 of this work.[13] The tracheidal pore channel system of wood with a preferential orientation in axial direction offers the possibility to use liquid infiltration techniques to transform the bioorganic wood structure into an inorganic ceramic material. After pyrolysis at 1800°C a porous carbon template of wood was obtained which was subsequently infiltrated with silion melt at 1600°C. The resulting cellular β-SiC ceramics contain a residual silicon content of 23–67 vol%. Table 1 summarizes the properties of the pyrolyzed and Si-infiltrated materials which were prepared from different kinds of wood. Representative microstructures of the pyrolyzed carbon preforms and the silicon infiltrated SiC-reaction products of the investigated kinds of wood are given in Ref. 13.

The microstructures of the carbonized preforms and the final porous ceramic materials were characterized by SEM (Stereoscan S 250 MK3, Cambridge Instruments, Cambridge, UK). Density and porosity were measured by Helium pycnometry (Accu Pyk 1330, Micromeretics, Dusseldorf, Germany).

Rectangular specimens of different orientation with respect to the initial cell structure were prepared from the carbonized wood preform and siliconized ceramic reaction product, respectively (Fig. 2). Elastic moduli were derived in different loading directions from stress–strainmeasurements in an Instron universal testing machine (4204, Instron, High Wycombe, Buckinghamshire, UK). Modulus of rupture (fracture strength) was measured by four point bending (20/40 mm) according to ASTM C 1161-90 using specimens of $5\times6\times60$ mm.[3] The loaded cross-section of the specimens was larger than the standard values (3×4 mm^2) to account for the meso- and macroscopic non-uniformity of the cellular structure of these materials. A loading

Table 1. Properties of carbon preform and Si-infiltrated SiC materials derived from various kinds of wood

Wood		*Balsa*	*Pine*	*Oak*	*Maple*	*Beech*	*Ebony*
Density ($g\,cm^{-3}$)	Pyrolyzed	0.06	0.31	0.50	0.51	0.55	0.87
	Si-infiltrated	2.02	2.22	2.16	2.58	2.57	—
Porosity (%)	Pyrolyzed	22170	21/57	30/40	43/22	42/21	23/20
(open/closed)	Si-infiltrated	11/14	11/14	8/5	3/5	3/2	3/—
Mean pore diameter*(μm)		40	20	170	35	30	—
Si-content (wt%)		67	50	27	23	37	—

*Open pore channels (tracheides) free of Si.

rate of 0·5 mm min^{-1} was applied and strain was deteced by an inductive strain gauge. Mean values of strength and elastic modulus were obtained from a minimum of 10 measurements. Compression strength was measured at the pyrolyzed carbon preform only using rectangular cubes of 15 mm according to DIN V ENV 12291. Fractured surfaces were analyzed by SEM.

3 Results

3.1 Pyrolyzed carbon preform

Figure 3 shows the elastic modulus and bending strength of the pyrolyzed carbon preform as a function of density for the two different loading orientations parallel (LT and LR) and perpendicular (TL and TR) to the axial direction. As expected from the mechanical behavior of wood,[1] Young's modulus and strength of the carbon preform are significantly higher in the axial direction compared to perpendicular loading orientations.

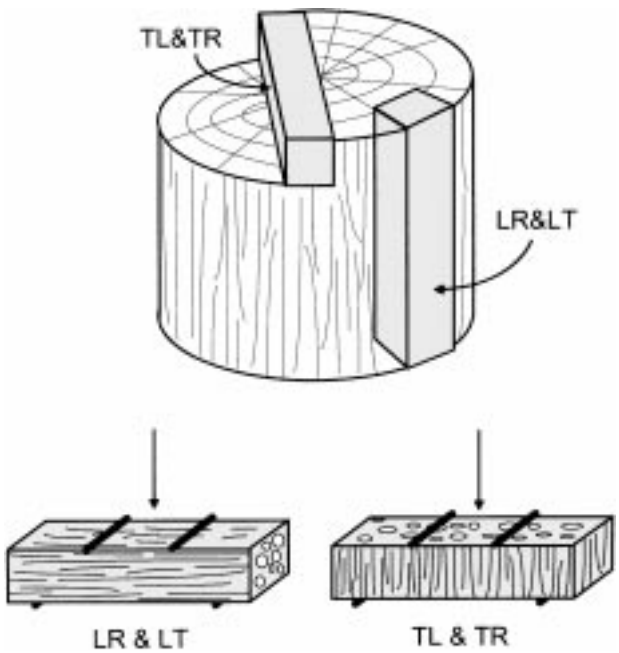

Fig. 2. Preparation of specimens and loading orientations for the mechanical property measurements.

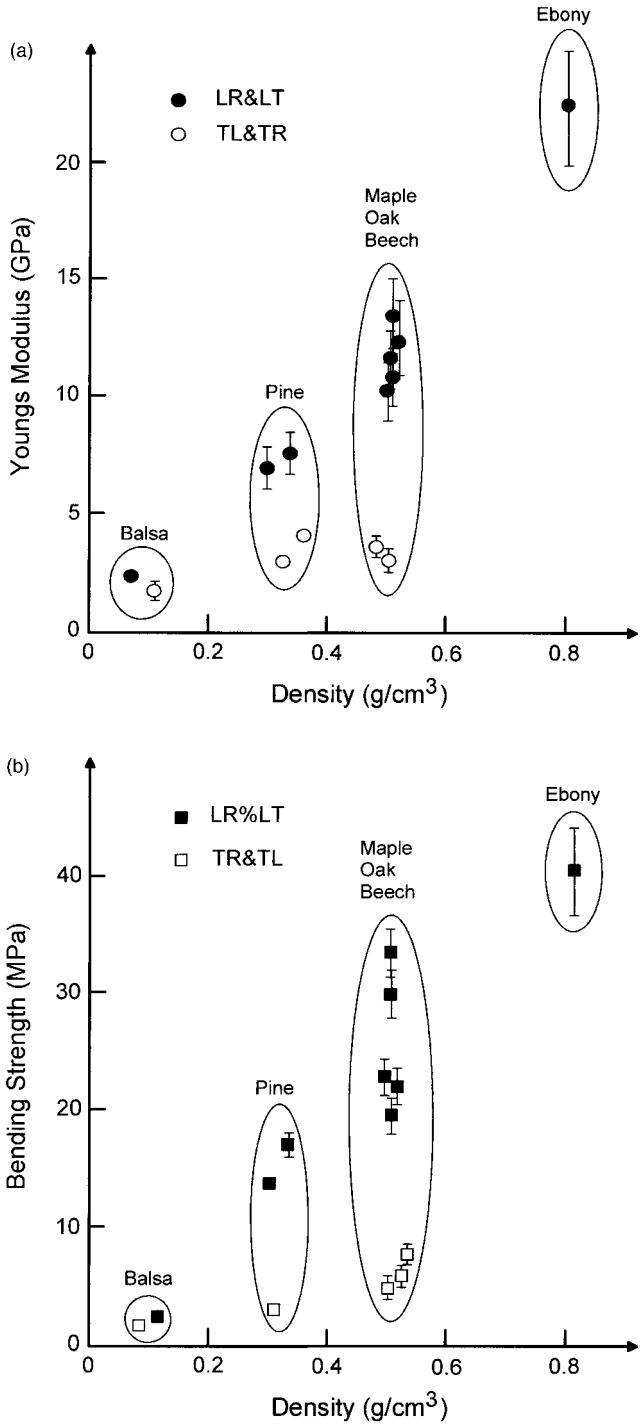

Fig. 3. Elastic modulus and bending strength of the pyrolyzed carbon preform as a function of density for the two different orientations parallel (LT and LR) and perpendicular (TL and TR) to the axial direction.

While pyrolyzed ebony with a density of 0·82 g cm^{-3} attains a Young's modulus of 22 GPa and a bending strength of (42 ± 7) NPa pyrolyzed balsa has a density of only 0·07g cm^{-3} and hence a very low Young's modulus of 2 GPa and a modulus of rupture of 2·5 MPa.

Stress–strain diagrams of pine and oak are shown in Fig. 4 together with the micrographs of corresponding fracture surfaces. The pyrolyzed wood preform achieves a strain-to-failure of 0·1–0·3%. Inhomogeneities in the stress–strain curve indicate a nonlinear fracture growth behavior which can be attributed to the macroscopic inhomogeneities of growth ring patterns in the cellular microstructure [(Fig. 4b)]. The fracture patterns are similar to those found in laminate composites[14] indicating an extensive change of crack propagation direction at the boundaries where large changes in fractional density occur.

Figure 5 shows the development of anisotropic deformation resistance under compression loading with increasing pyrolysis temperature for the example of maple. From a pyrolysis temperature of 600°C up to 1800°C XRD proved that the

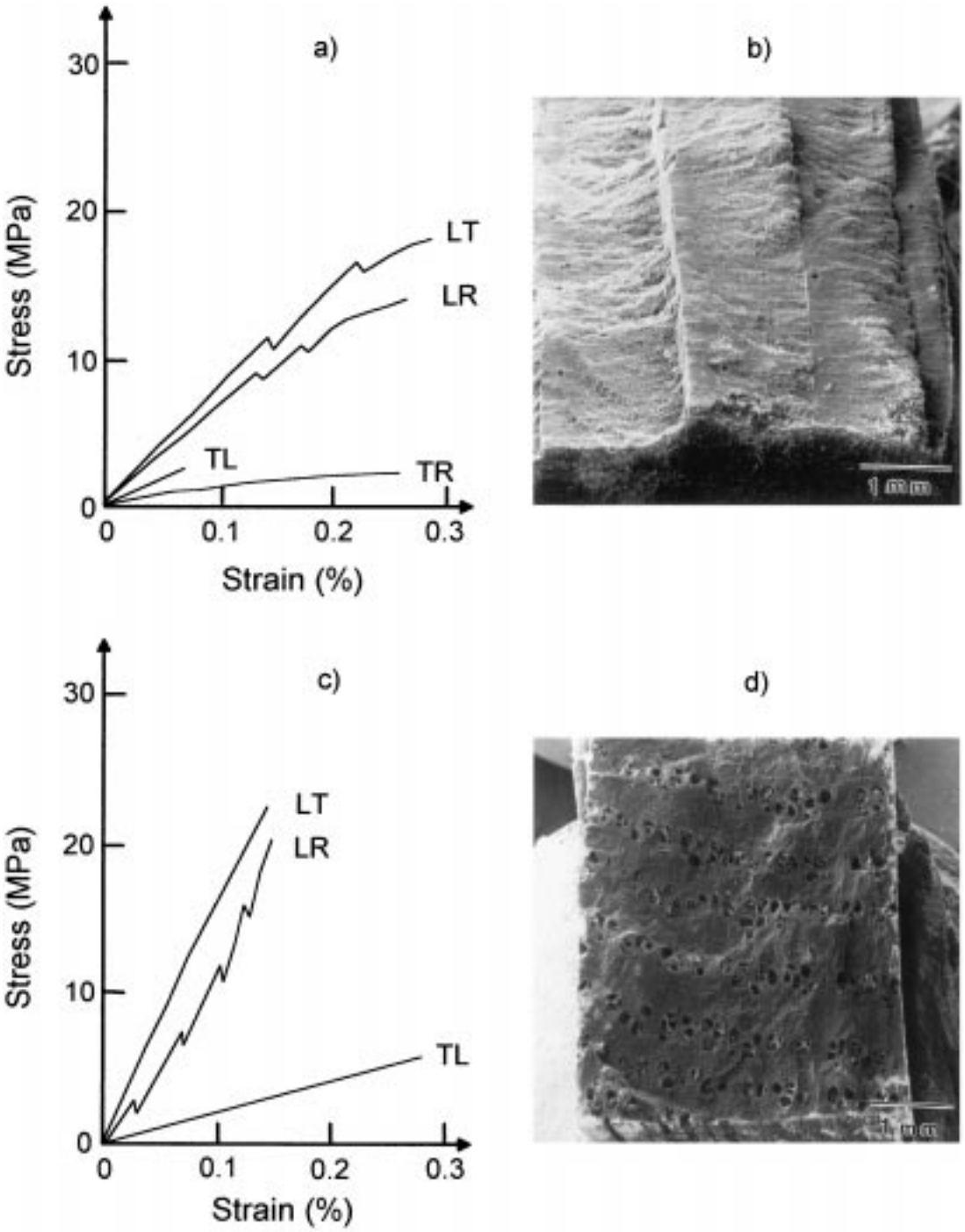

Fig. 4. Stress–grain diagrams of pine (a) and oak (c) pyrolyzed at 1800° together with the micrographs of corresponding fracture surfaces.

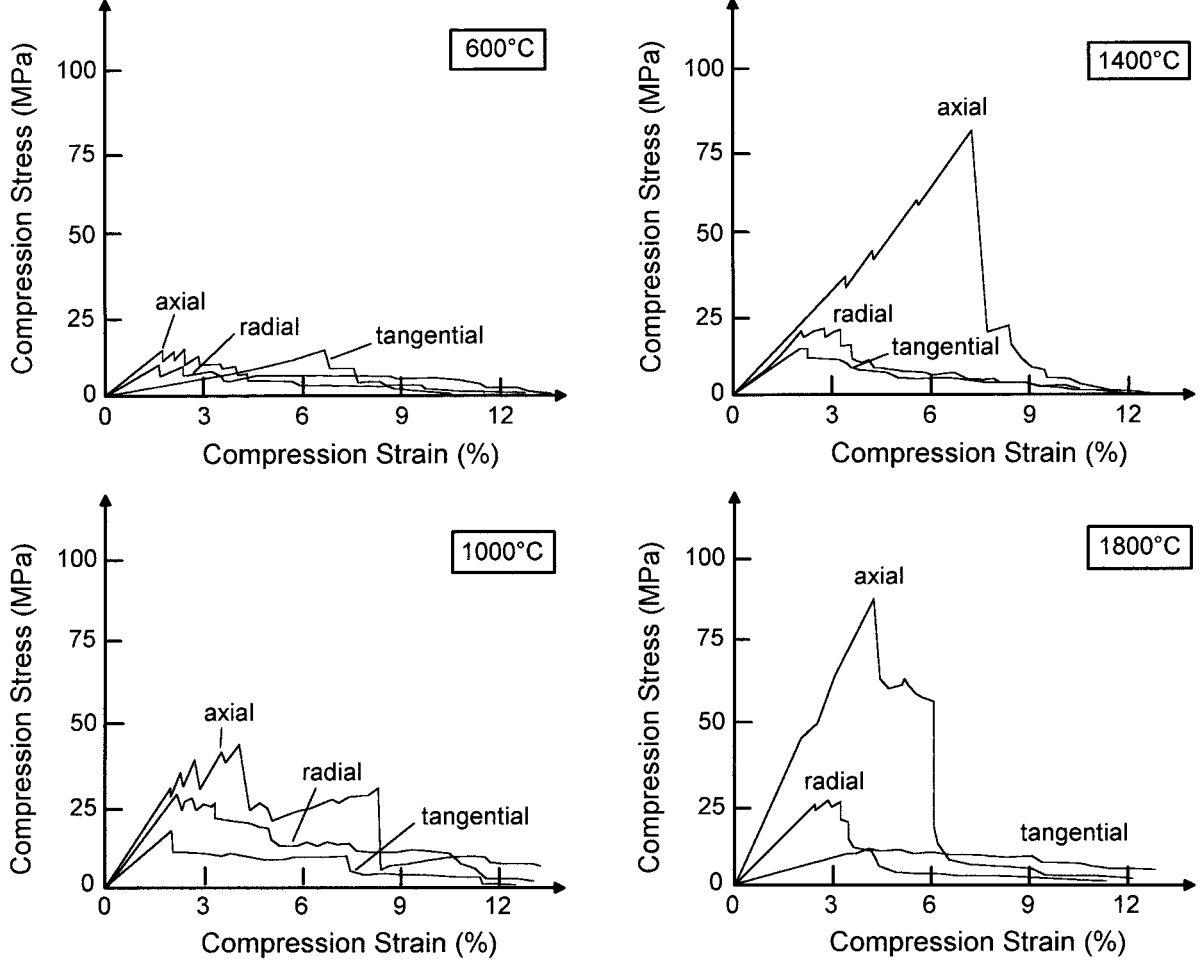

Fig. 5. Development of anisotropic deformation resistance of maple under compression loading with increasing pyrolysis temperature for the example.

crystallinity of the carbon resulting from the thermal induced decomposition of the polyaromatic biopolymers increases to a more graphitic like microstructure at the highest temperature.[13] Simultaneously the strain-to-failure under compression is reduced from approximately 12 to 6% in axial direction whereas the compression strength increases from 15 to 85 MPa. Total porosity at all pyrolysis temperatures remains almost constant at 70%.

3.1.1 Silicon infiltrated SiC-reactron product

Figure 6 shows the elastic modulus and bending strength of the silicon infiltrated SiC-reaction products as a function of density. Due to the silicon infiltration the density is significantly higher compared to the highly porous carbon preform materials. The differences between the LT/ LR directions and TLTR directions can still be found even though they are less pronounced compared to the carbon preform materials shown in Fig. 4. For example, maple has a strength of 120 MPa in TL and TR directions whereas fracture stress in LR and LT directions attains 200 MPa at a density of 2·5 g cm^{-3} (porosity 8%).

Stress–strain diagrams of silicon infiltrated SiC derived from oak and pine are shown in Fig. 7. Compared to the fracture behavior of the pyrolyzed preforms the ceramic materials achieve a smaller strain-to-failure but a significantly higher fracture stress. The specimens loaded in TL and TR directions behaved in linear elastic fashion until catastrophic failure occurred at a strain-to-failure of less than 0·06%. Significantly higher failure strains up to 0·12% were found in specimens loaded in the LR and LT directions. Specimens loaded in these directions also deformed in a linear elastic fashion until a critical yield stress at approximately 100–110 MPa was reached, at which point crack growth began. However, rather than travelling right across the specimen the crack was deflected from the propagation direction resulting in a waved and graduated fracture surface similar to the pyrolyzed carbon preform material.

4 Discussion

For porous ceramic materials a variety of emperical relations were derived to account for the

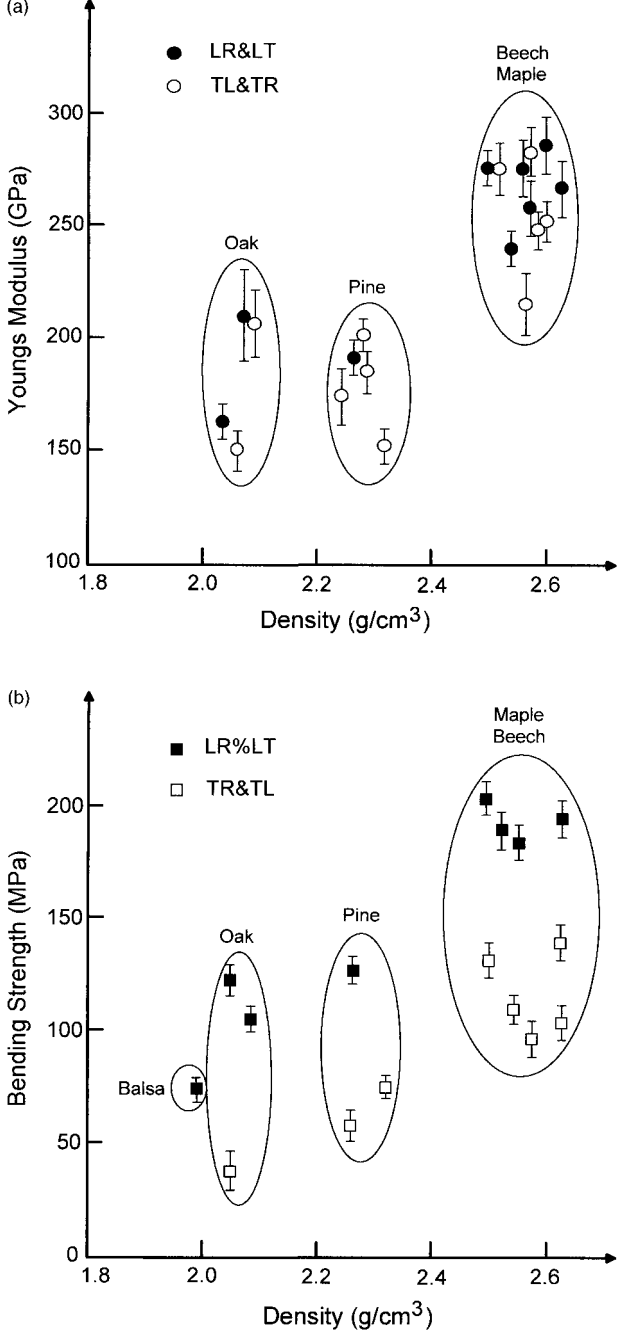

Fig. 6. Elastic modulus and bending strength of the Si-infiltrated SiC-reaction products as a function of density.

influence of pore fraction and pore shape on the strength and failure behavior under tensile as well as under compressive stresses.[15–19] In the case of non-interacting pores, e.g. at lower porosity levels pore size and pore size distribution were considered to exert a major influence on the strength.[20,21] The mechanical properties of highly porous brittle structures such as ceramic honeycombes and foams were shown to depend on the cellular structure size (cell size) and the variation of strength distribution in the solid material (expressed by the Weibull factor).[22,23]

Relations based on the minimum solid area model are commonly used to describe a fractional strength (strength of the porous over strength of the completely dense material) as an exponential function of the pore volume fraction over a wide range of porosities[16]

$$\sigma^* = \frac{\sigma_p}{\sigma_s} = \exp(-AV_p) \tag{1}$$

The total porosity V_p in the solid can be expressed in terms of a fractional density ρ^*

$$V_p = 1 - \rho^* \tag{2}$$

with ρ^* being the ratio of the geometrical density of the porous compact over the density of the fully dense solid material ($\rho^* = \rho_p/\rho_s$ where ρ_s was taken as $1{\cdot}5\,\mathrm{g\,cm^{-3}}$ for pyrolytic C and 2·6–3·1 $\mathrm{g\,cm^{-3}}$ for Si–SiC depending on the Si content, respectively) Hence

$$\sigma^* = \exp[A(\rho^* - 1)] \tag{3}$$

where A is a constant which often was found to equal 5 for spherical pores and higher values for elongated pore shape. Using eqn (3) the bending strength (in axial direction) of the pyrolyzed carbon preform and the Si-infiltrated SiC ceramic product drawn in Fig. 8 can be described with $A = 4$ in axial and $A = 5{\cdot}5$ in radial and tangential loading directions (σ_s was taken as 300 MPa for carbon and 350 MPa for Si–SiC, respectively). For comparison data of three point bending strength measurements of porous Si–SiC ceramics prepared by Si-infiltration of a SiC powder (mean particle diameter 69 μm)/carbon powder mixture (SiC/C as 95/5 by weight)[24] are also given in Fig. 8. The Si–SiC derived from wood exhibits a higher strength at the same porosity level (and a similar mean pore size of 10–20 μm) when it was loaded in axial direction.

Measurements of bending strength, Youngs modulus and strain to failure as a function of loading direction show a pronounced anisotropic material behavior. Assuming constant properties of the cell wall material the anisotropic mechanical properties of wood were described by a cellular model.[5] For a highly porous cellular solid fractional Young's modulus $E^*(= E_pE_s)$, compressive strength $\sigma^*_{\mathrm{comp}}(=\sigma_p/\sigma_s)$ as well as other properties such as Poisson ratio, fracture toughness, etc. can be expressed by

$$E^* = C(\Phi\rho^*)^n + C'(1 - \Phi)\rho^* \tag{4}$$

Φ represents the fraction of open porosity to closed porosity and defines the range of validity for the open cell (OCF) and closed cell (CCF) modifications of the cellular model at $\Phi \rightarrow 1$ and

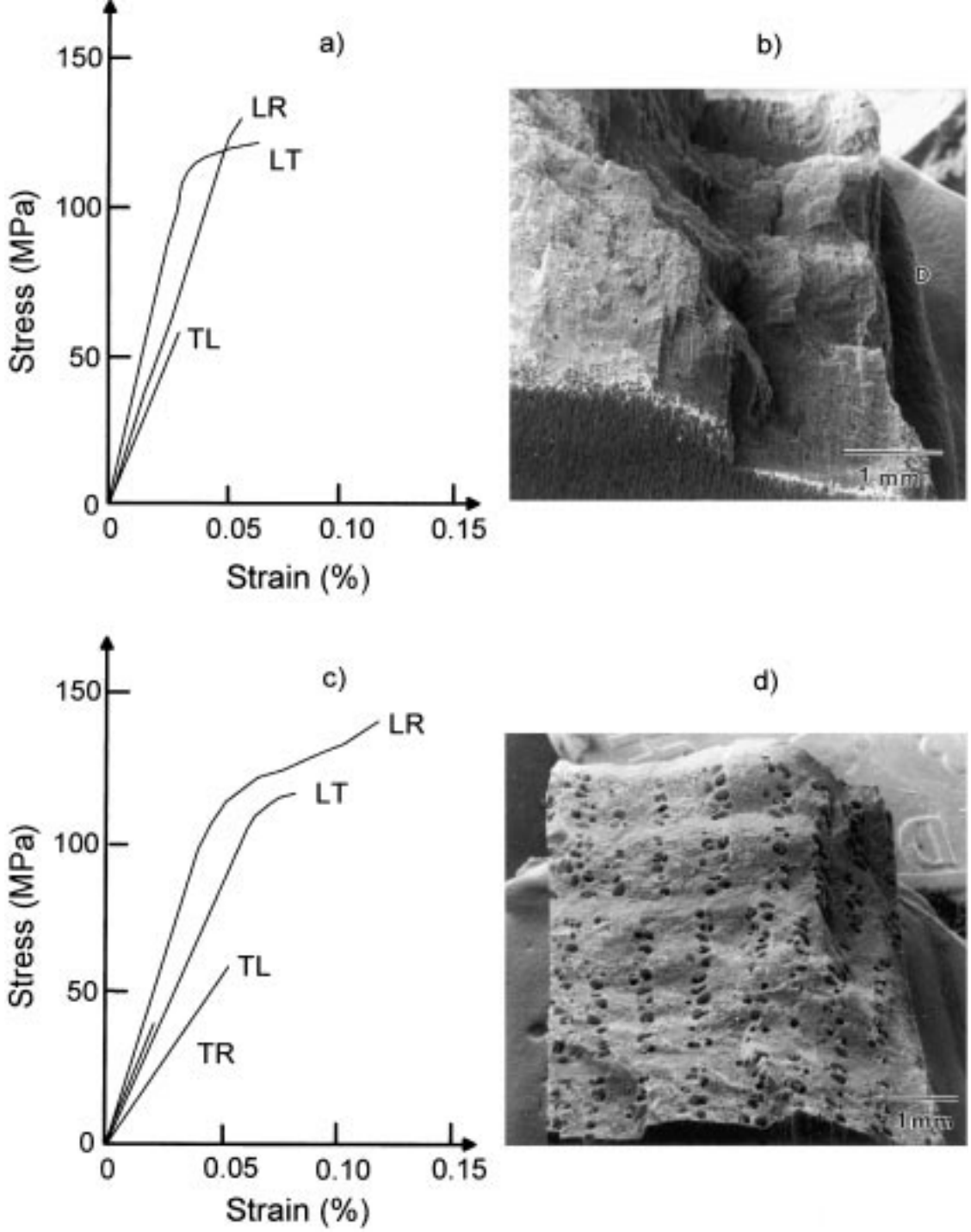

Fig. 7. Stress–strain diagrams of silicon infiltrated SiC derived from oak and pine.

$\Phi \approx 0{\cdot}6$–$0{\cdot}8$, respectively. C, C' and n are constants which depend on the loading direction with respect to the cellular pore orientation. While for axial direction n was found to be 1 for various kinds of wood higher values of $n = 2$ (strength) and 3 (elasticity) were obtained for the tangential and radial directions.[5] Thus, loading perpendicular to the cell walls generally shows a significantly higher sensivity to porosity level as compared to the axial loading direction.

In contrast to the bending strength, evaluation of the Young's modulus–density relation indicates no significant difference between the various loading directions (Fig. 9). The highly porous carbon preform as well as the Si infiltrated SiC can be fitted by eqn (4) using $\Phi = C = 1$ and $n = 2$. For the Young's moduli of the dense solid material, E_s, a value of 100 GPa was taken for carbon and 370–230 GPa for Si–SiC depending on the Si-content, respectively. The higher sensivity of bending strength compared to the elasticity on the microstructural anisotropy may be attributed to the role of the large tracheidal pores for failure initiation in the Si-infiltrated SiC material. For the case of LR

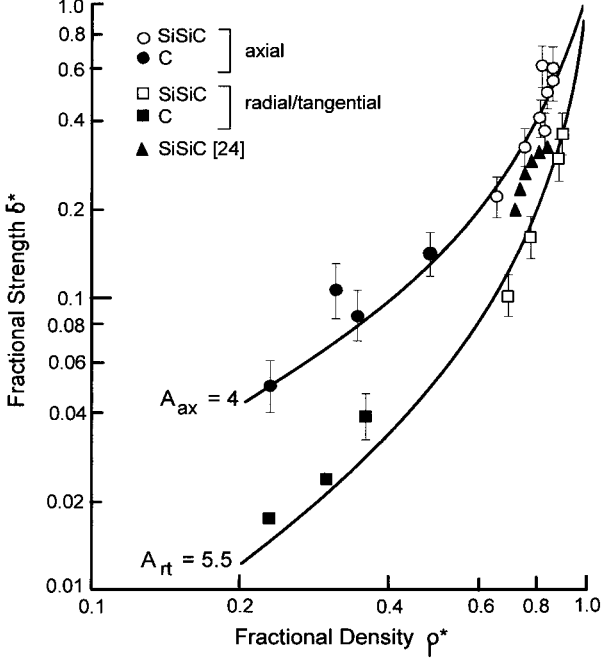

Fig. 8. Fractional bending strength as a function of density in the pyrolzed carbon preform and the Si-infiltrated SiC ceramic. The data were fitted with eqn (4).

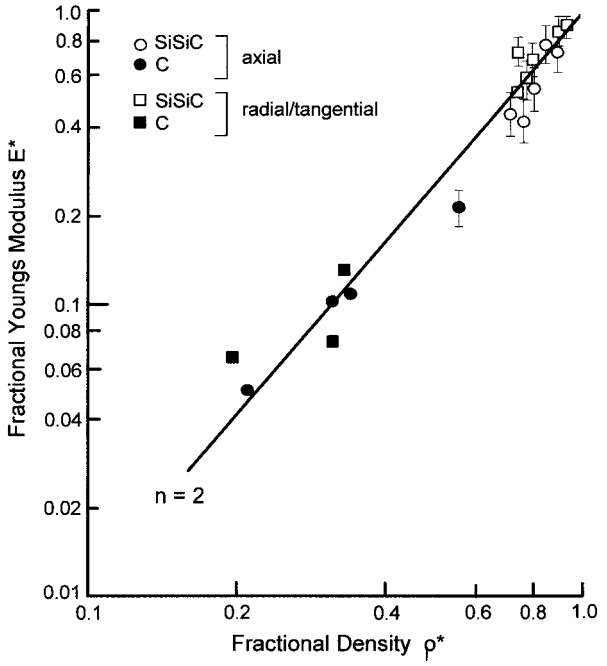

Fig. 9. Fractional Young's modulus versus fractional density of pyrolyzed carbon preform and Si-infiltrated SiC. The data were fitted with eqn (5).

and LT loading directions the large unfilled tracheidal pores are oriented perpendicular to the normal tensile stress and will act as crack initiation sites when a critical loading stress is reached. Crack propagation is suggested to be localized in a plane with high pore density where the crack can easily propagate parallel to the pore channel orientation and the Si–SiC interface (Fig. 10). Due to the small fraction of load bearing Si–SiC material bridges

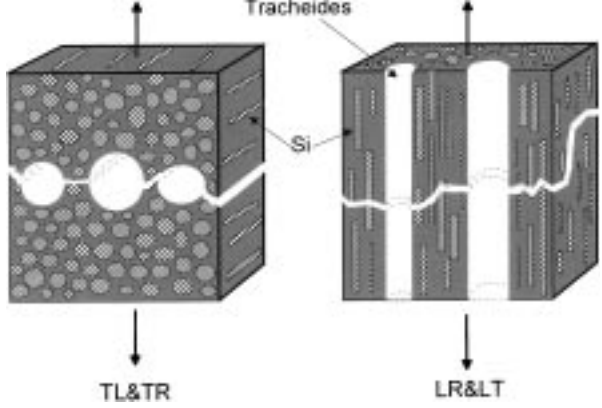

Fig. 10. Model of crack progagation as a function of loading directions versus pore orientation.

catatrophic failure at low fracture stresses and strains occur. For loading directions parallel to the tracheidal pore system, however, undulations of low and high density regions result in a variation of crack resistance in the crack extension direction. The macroscopic growth ring patterns give rise for crack deflection which is confirmed by the fracture surface morphology and the non-linear stress–strain curves.

Strength of porous Si–SiC derived from wood is dominated by the size distribution and the orientation of the tracheidal pore channels. The large tracheidal pores remain unfilled of silicon whereas pores with a diameter less than approximately 20 μm were completely filled with residual silicon. Wood with a small fraction of large tracheidal cells such as pine and other coniferous wood can be used to fabricate Si–SiC ceramics of high density and hence improved strength and stiffness in the axial direction. Wood with a high fraction of large pore channels may be interesting for porous Si–SiC materials which show a low stiffness but a high damping capacity in a loading direction perpendicular to the pore channel extension. When the residual silicon is removed by chemical etching SiC materials with a porosity in the range of that of the pyrolyzed preform can be obtained. Due to a small SiC particle size of less than 5 μm a high internal surface is generated. Such anisotropic porous structures may be of particular interest for a variety of high temperature processes such as hot gas purification, heat exchange devices, catalyst carriers, etc.

5 Conclusions

Silicon infiltrated silicon carbide ceramics with anisotropic pore orientation were fabricated from carbon preforms which were obtained from pyrolyzed wood. While the mechanical behavior of the

pyrolyzed carbon preform material can be described according to the cellular model as for wood the lower porosity in the final ceramic material results in a less degree of anisotropy. Generally, the mechanical properties in axial loading direction are superior to the properties in perpendicular loading directions which are much more sensitiv to porosity variation. Compared to conventionally fabricated ceramics of the same overall phase composition but isotropic porosity distribution the biogenetic Si–SiC ceramics are distinguished by a higher strength (in axial direction) at the same level of porosity. Biogenetic ceramics with anisotropic porosity may be of increasing interest for the development of novel light weight high temperature resistant materials. Light weight ceramics with low density but high strength and corrosion resistance are candidates for applications where anisotropic behavior is used such as in filters, catalyst carriers, heat insulation structures, etc.

References

1. Ashby, M. F., Easterling, K. E., Harrysson, R. and Maiti, S. K., The fracture and toughness of woods. *Proc. Roy. Soc. London*, 1985, **A 398**, 261.
2. Ashby, M. F., On the engineering properties of materials. *Acta Metall.*, 1989, **37**, 1273.
3. Ashby, M. F., Materials and shape. *Acta Metall.*, 1991, **39**, 1025.
4. Desch, H. E. and Dingwoodie, J. M., *Timber*, McMillan, New York, 1981.
5. Gibson, L. J. and Ashby, M. F., *Cellular Solids, Structure and Properties*, Pergammon Press, New York, 1988.
6. Hagiwara, H. and Green, D. J., The mechanical behavior of lightweight cellular ceramics. *Advanced Ceramics II*, Elsevier Publishers London, 1986, p.105.
7. Brezny, R. and Green, D. J., Fracture behavior of open-cell ceramics. *J. Am. Ceram. Soc.*, 1989, **72**, 1145.
8. Brezny, R. and Green, D. J., The effect of cell size on the mechanical behavior of cellular materials. *Acta Metall.*, 1990, **38**, 2517.
9. Brezny, R. and Green, D. J., Mechanical behavior of cellular ceramics. Chapter 9 *Materials Science and Technology*, Vol. 11 VCH Verlag Weinheim/Germany, 1994, p. 463.
10. Gibson, L. J. and Ashby, M. F., Hierarchical cellular materials. *Mat. Res. Soc. Symp. Proc.*, 1992, **255**, 343.
11. Gibson, L. J., Wood: a natural fibre reinforced composite. *Metals and Materials*, 1992, **8**, 333.
12. Knigge, W. and Schulmi, H., *Grundriss der Forstbenutzung*, Verlag Paul Parey, Hamburg/Germany, 1966.
13. Greil, P., Lilka, T. and Kaindl, A. Biomorphic cellular silicon carbide ceramics from Wood: I. Processing and microstructure. *J. Eur. Ceram. Soc.*, 1998, **18**, 1961.
14. Clegg, W. J., The fabrication and failure of laminar ceramic composites. *Acta Metall.*, 1992, **40**, 3085.
15. Ryshkewitch, E., Compression strength of porous sintered alumina and zirconia. *J. Am. Ceram. Soc.*, 1953, **36**, 65.
16. Rice, R. W., Microstructure dependence of mechanical properties of Ceramics. *Treatise on Materials Science and Technology*, 1, **11**, 199.
17. Wagh, S., Singh, J. P. and Poeppel, R. B., Dependence of ceramic fracture properties on porosity. *J. Mat. Sci.*, 1993, **28**, 3589.
18. Brezny, R. and Green, D., Mechanical behavior of cellular ceramics. In *Materials Science and Technology*, ed. R. W. Cahn, P. Haasen and E. J. Kramer. Vol. 11, *Structure and Properties of Ceramics*, ed. M. S. Swain, Wiley-VCH, New York, 1994, p. 465.
19. Boccacini, A. R., Bossert, J., Wicker, M. and Mombello, E. E., Calculation of strength of porous materials by Consideration of Flaw Stresses. *Materialwissenschaflen und Werkstofftechnik*, 1997, **28**, 1 (in German).
20. Vardar, Ö. and Finnie, I., Effect of spherical pores on the strength of a polycrystalline ceramic. *Int. J. Fracture*, 1977, **13**, 215.
21. Luping, T., A study of the quantitative relationship between strength and pore size distribution of porous materials. *Cement and Concrete Research*, 1986, **16**, 87.
22. Huang, J. S. and Gibson, L. J., Fracture Toughness of Brittle Honeycombes. *Acta Metallurgica et Materialia*, 1991, **39**, 1617.
23. Huang, J. S. and Gibson, L. J., Fracture toughness of brittle foams. *Acta Metallurgica et Materialia*, 1991, **39**, 1627.
24. Osada, H., Kani, A., Katayama, S. and Koga, T., Bending strength and electric resistivity of porous Si–SiC ceramics. In *Ceramic Transactions*, Vol. 31, *Porous Materials*, ed. K. Ishizaki. The American Society, 1993, p. 243.